ACS Catalysis

pubs.acs.org/acscatalysis Research Article

Pulsing the Applied Potential in Electrochemical CO_2 Reduction Enhances the C_2 Activity by Modulating the Dynamic Competitive Binding of *CO and *H

Rileigh Casebolt DiDomenico,[§] Kelsey Levine,[§] Colin Bundschu, Laila Reimanis, Tomas Arias, and Tobias Hanrath*

Cite This: *ACS Catal.* 2024, 14, 785−796 Read Online

ACCESS | Metrics & More | Article Recommendations | Supporting Information

ABSTRACT: We explore dynamic electrocatalysis by pulsing the applied potential to modulate the temporal microenvironment during the electrochemical reduction of CO_2. We focus on copper electrodes by virtue of their unique ability to bind *CO intermediates and enable C−C coupling to form high-value C_2 products, such as ethylene or ethanol. We examine the well-known competition between *CO and *H for active sites, as their relative coverage is crucial for enhancing the formation of C_2 products. We found that pulsing the applied potential can significantly enhance the electrocatalytic activity of C−C coupling, increasing the turnover frequency of C_2 products by up to 33-fold compared to potentiostatic electrolysis. We interpret this improvement in the context of oscillating surface coverage and the transient dynamics of the *CO/*H coverage during the cathodic pulse. Through a combination of experimental and computational methods, we investigate how pulse frequency influences the turnover frequency of CO_2 to C_2 products on Cu. Our study not only validates recent theoretical predictions about the potential of dynamic (electro)catalysis to surpass the limitations imposed by the Sabatier limit but also uncovers scientific and mechanistic insights into dynamic processes within the electrical double layer. These insights are instrumental in formulating design principles for pulsed CO_2 electrolysis with enhanced C_2 activity. The outcomes of this study lay a foundational framework for future advances in programmable CO_2 electrolysis with improved activity, selectivity, and durability.

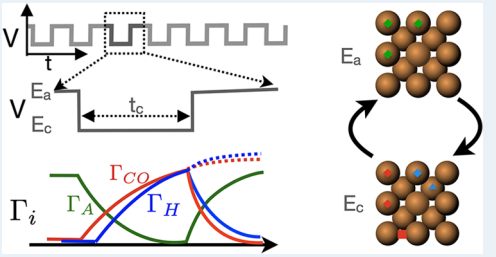

KEYWORDS: *pulsed electrochemical CO_2 reduction, dynamic catalysis, turnover frequency, competitive adsorption, copper electrode*

INTRODUCTION

Driven by growing concerns about the effects of anthropogenic CO_2 emissions on the now evident impacts of global climate change, the electrochemical CO_2 reduction reaction (CO_2RR) has emerged as a promising approach to transform CO_2 from an environmental liability to a feedstock for chemical products.[1,2] A central aim of CO_2RR research is to direct the heterogeneous electrocatalytic reaction toward the formation of specific high-value C_2 products (e.g., ethylene), which is an attractive target for meaningful global warming impact reduction due to its large global market size.[1] Among the various electrocatalysts that have been examined for the CO_2RR, copper has emerged as one of the best due to its ability to bind *CO and other important CO_2RR intermediates that lead to high C_2 activity.[3]

In the context of enhancing C−C coupling to increase the C_2 activity, the key reaction pathways are shown in Figure 1a. Importantly, the C−C coupling competes with the H−H coupling to form H_2 (hydrogen evolution reaction (HER)). Thus, a strategy for enhancing C−C coupling and C_2 activity is to manage the coverage of adsorbed carbon monoxide intermediates (*CO) and adsorbed hydrogen (*H) species[4] and to minimize other competitive reactions including the hydrogen evolution reaction (HER), C_1, and CO oxidation pathways.[5] A recent review by Xiang et al. summarized key approaches to boosting CO_2RR toward C_{2+} products by balancing *CO and *H via methods to modify the microenvironment near the active site (e.g., composition, structure promoters, etc.).[4] Beyond the realm of these "static" parameters, the concept of a "dynamic microenvironment" (e.g., programmable oscillations in applied potential, temperature, or pressure) has recently emerged as a promising avenue to investigate and optimize coupled reaction and transport processes within the microenvironment.[6,7]

Pulsing the applied potential presents an attractive and versatile approach to modify the temporal microenvironment and dynamically control the *CO and *H surface potential,

Received: September 6, 2023
Revised: December 19, 2023
Accepted: December 19, 2023
Published: January 3, 2024

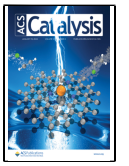

https://doi.org/10.1021/acscatal.3c04224
ACS Catal. 2024, 14, 785−796

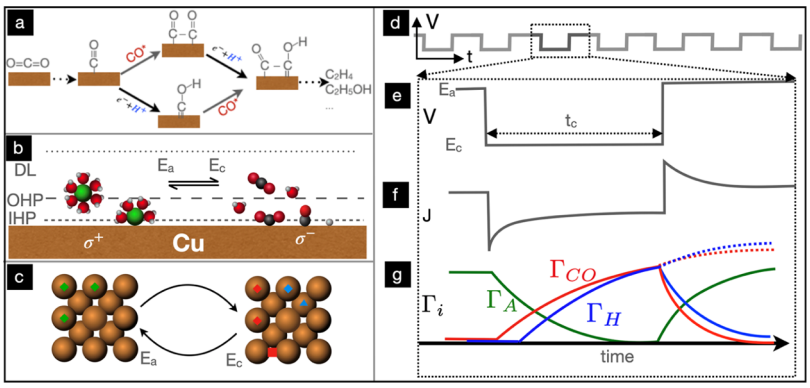

Figure 1. (a) Simplified electrochemical CO_2 reduction pathway to C_2 products focusing on C−C coupling via the Langmuir−Hinshelwood mechanism (top, dimerization) or the Eley−Rideal mechanism (bottom, insertion). (b) Schematic of dynamic changes at the electrode/electrolyte interface including ion distribution within the electrical double layer during oscillation between the anodic and cathodic applied potential. (c) Surface coverage of species on the Cu(100) surface in response to the oscillating cathodic and anodic applied potential. Anions (green) are adsorbed on the surface under anodic conditions, and *CO (blue) and *H (red, atop, and hollow) are adsorbed under cathodic conditions. (d) Pulsed potential profile. (e) Zoomed-in potential step from the anodic (E_a, upper) potential to the cathodic (E_c, lower) potential for a specified pulse duration. (f) Corresponding current response to the cathodic potential step. (g) Illustration of transient surface coverage of the competing *H, *CO, and adsorbed anions *A.

thereby changing the binding affinity and surface coverage of different reaction intermediates. Considering the fact that heterogeneous electrocatalytic reactions involve a sequence of coupled subprocesses, modulating the potential impacts of the spatiotemporal concentration gradients, distribution of bound adsorbates and intermediates, and consequently, reaction pathways and product selectivity.[8,9]

The emerging mechanistic understanding is that changing the applied potential provides a way to control the distribution of species bound to the catalyst surface. For example, in the context of CO_2RR, pulsing is advantageous since it suppresses the undesirable HER side reaction in addition to prolonging the electrode lifetime by preventing deactivation from contaminating species.[10−15] Pulsing also modifies reaction selectivity by dynamically changing the reaction environment through electrode modification (oxidation and reconstruction), double-layer rearrangement, and species adsorption.[16−27] Large potential swings affect the electric field at the surface, resulting in significant non-Faradaic and Faradaic currents, which impact local electric fields and reaction selectivity.[28,29] Beyond studying the impact of pulsing on selectivity and durability, relatively less work has been done to examine how activity is impacted by pulsing.

Recent theoretical studies have examined the concept of breaking beyond the limits of the Sabatier principle by conducting the reaction in periodic modulation between the weakly and strongly bound states, thereby enabling catalytic activities that surpass the rates attainable in "static" microenvironments.[30] An initial validation of this concept was provided by the experimental study of Gopeesingh et al.,[31] who demonstrated significant enhancement of formic acid oxidation rates via pulsed potential catalytic resonance where the lower potential favored the non-Faradaic *CO formation pathway and the upper potential favored the Faradaic oxidation. A more recent theoretical study by Baz et al.[32] showed that in the specific case of electrocatalytic reactions, changing the applied potential is distinct from changing the binding energy of specific intermediates because the potential changes the free energy of the reaction for all steps equally. Their analysis showed that the turnover frequency of simple electrocatalytic reactions (e.g., a series of electrochemical steps) does not benefit from the pulsed modulation of the applied potential. However, for more complex reaction environments (e.g., involving two competing parallel reactions with a site-blocking species), the application of a pulsed potential can enhance the overall activity of the reaction.

Inspired by recent theoretical predictions and concurrent experimental advances in potentiodynamic catalysis, we set out to examine how pulse frequency (PF) impacts the turnover frequency (TOF) of CO_2 to C_2 products on Cu. We combined experiments and computational models to show how oscillating applied potentials impact the balance of the dynamic competition between *CO and *H for active sites on the copper electrode. Our results enable future advances in pulsed electrochemical CO_2RR by providing mechanistic insights and design principles for optimal square-wave pulse profiles toward efficient CO_2 to C_2 transformation pathways.

RESULTS AND DISCUSSION

Dynamic Electrocatalysis and Interfacial Processes. The electrochemical transformation of CO_2 to CO intermediates and the subsequent C−C coupling to form C_2 products (e.g., C_2H_4 or C_2H_5OH) involves a sequence of linked subprocesses that span multiple lengths and time scales. As shown in Figure 1, this sequence begins with the transport of CO_2 from the bulk electrolyte through the diffusion boundary layer and the electrical double layer (EDL). CO_2 then adsorbs onto an active site on the Cu electrocatalyst surface, where it is transformed through a series of electron and proton transfer reactions to form reduced intermediates and products that subsequently desorb from the surface. Notably, each subprocess in this sequence is associated with a characteristic rate. Therefore, periodic modulations of the experimental conditions (e.g., pulsing the applied potential with a specific frequency) present an opportunity to understand and control the dynamic interplay of the transport and reaction subprocesses. In this context, we sought to understand the fundamental relationship between the applied pulse frequency (PF) and the turnover frequency (TOF) of the competing reactions to form C_2 products and H_2.

To systematically examine pulsed electrolysis of CO_2, we focused on pulse profiles that allowed us to untangle the

https://doi.org/10.1021/acscatal.3c04224
ACS Catal. 2024, 14, 785−796

dynamic response of the "hard" (i.e., copper surface) and "soft" (i.e., EDL and diffusive layer) side of the electrode/electrolyte interface. The prevailing electrochemical conditions can lead to variations in composition (oxidation state) and structure (macroscopic roughness and microscopic surface reconstruction). For instance, Timoshenko et al. found that copper oxides are generated at ∼0 V vs Ag/AgCl in 0.1 M $KHCO_3$ when the anodic pulse duration is at least 0.5 s.[33] A similar pulsed CO_2 electrolysis study by Kimura et al. showed that in 0.1 M $KHCO_3$, oxidation of the copper electrode occurs if the anodic pulse potential is more positive than 0 V vs Ag/AgCl.[25] In the case of relatively long anodic pulses (i.e., t_a = 5 s at E_a= −0.18 V vs Ag/AgCl), the surface morphology of the copper electrode may change significantly.[34] However, in the case of shorter pulses (E_c = −1.6 V, E_a = 0 V vs Ag/AgCl, t_a = t_c = 1s, 0.1 M $KHCO_3$), Tang et al. showed that the copper electrode structure does not undergo significant changes in roughening or surface faceting.[26] In the experiments discussed below, we limited the anodic potential pulse to −0.2 V vs Ag/AgCl (significantly below the oxidation potentials reported in the literature) with pulse durations in the range of 50−500 ms. With the above-mentioned aspects in mind, we designed the pulse conditions examined in this study to explicitly avoid morphological or compositional changes in the copper electrode, focusing on examining C_2 activity trends in the context of dynamic changes within the electrolyte microenvironment.

The CO_2 concentration profile within the diffusive boundary layer near the copper electrode is significantly impacted by pulsing the applied potential in electrochemical CO_2 reduction.[35] During the cathodic pulse, the concentration of CO_2 is reduced, causing a decrease in its concentration within the boundary layer. However, during the anodic pulse, the CO_2RR ceases, and the CO_2 concentration near the electrode surface recovers. While transport effects are sometimes regarded as a nuisance in computational models,[36] pulsing puts transport effects under carefully controlled conditions, which allows us to better understand the dynamic interplay of transport, adsorption, and surface reactions to establish a more holistic picture of the heterogeneous catalytic process. We examined the spatial and temporal CO_2 gradients within the boundary layer using finite element simulations (Supporting Information S1). Pulsing the applied potential impacts the CO_2 concentration profile in two important ways: (i) the applied potential creates a microenvironment in which the time-averaged CO_2 concentration is higher than in comparable constant potential conditions and (ii) the amplitude of the CO_2 variation during each pulse scales in proportion to the duration of the pulse.

The dynamic changes within the EDL in response to the pulsed potential are more intricate. The identity and concentration of ionic species in the inner and outer Helmholtz layers (IHL and OHL) are subject to ongoing computational and experimental research.[37−40] To a first approximation, we assume that the reversal of electrode polarity during the pulse cycle is accompanied by a corresponding switch in the ionic nature of species within the EDL.[37] During the cathodic pulse, the negative electrode bias prompts an enrichment of solvated and bound cations in the EDL, whereas anions are depleted. The opposite electrostatic effects occur during the anodic pulse. However, the rate at which the EDL can rearrange in response to the applied potential pulse modulations is more complex. Figure 1g provides a qualitative depiction of the hypothesized transient surface coverage of hydrogen (*H), carbon monoxide (*CO), and anionic species (*A, representing hydroxide, chloride, carbonate, and bicarbonate). Pulsing the applied potential has two significant implications for the ionic species within the EDL. First, the anionic adsorbates, which form during the preceding anodic pulse, significantly influence the microenvironment. Prior research indicates that the control of oxygen-bound intermediates and the creation of a hydroxide (OH)-rich microenvironment can enhance carbon−carbon (C−C) coupling.[25,41−43] Second, during the cathodic pulse, hydrogen and carbon monoxide are involved in a dynamic competition for surface sites on the copper electrode. Consequently, the *CO/*H ratio will evolve during the cathodic pulse, and we hypothesized that systematic variations of the pulse duration will allow us to explore electrocatalysis in dynamic microenvironments with transient *CO/*H ratios that are unattainable under potentiostatic conditions.

Relationship between Pulse Frequency and Turnover Frequency. We investigated the effects of varying pulse frequency (PF = $(t_a + t_c)^{-1}$) on reaction activity, specifically toward C_2 products (ethylene and ethanol). We focused on symmetric square-wave potential modulations defined by a cathodic pulse at E_c = −1.65 V and an intermittent anodic pulse at E_a = −0.2 V vs Ag/AgCl. The experiments described below were performed using polycrystalline copper electrodes with Cu(100) dominated facets, as evidenced by the X-ray diffraction (XRD) patterns provided in the Supporting Information (SI, Figure S2).[11,26] The experimental trends summarized in Figure 2 reveal the impact of the pulse-modulated potential on product distribution. The constant potential reference condition (−1.65 V) yields a C_2 Faradaic efficiency (FE) of ∼34% after 10 min of electrolysis, which is comparable to values reported in the previous literature.[12,28,44] Notably, after extended potentiostatic electrolysis time (i.e., 2 h), the average C_2 FE drops to 14% (Figure 2a). Pulsing suppresses the 2 h average of the competing HER FE from ∼59% in potentiostatic electrolysis to below ∼20% at all pulse frequencies tested. Concurrently, pulsing enhances C_2 FE from 14% under potentiostatic conditions to 74, 76, and 53% at PF = 0.1, 1, and 10 Hz, respectively.

To describe the experimental trends in terms of intrinsic catalytic activity, we translated the partial current densities to turnover frequencies (TOF), as shown in Figure 2b. TOF measures the catalyst activity, defined as the number of turnovers of the catalytic cycle with respect to a specific product per time per active site.[45] Accurate TOF and catalytic activity data are essential to interpret and compare experimental and computational data for catalyst development.[36,46] To obtain an accurate and reliable measure of the TOF, the measured current density has to consider parasitic reactions, real (i.e., electrochemically active) surface area, series resistance, capacitive behavior, and other noise factors. To account for these aspects, Anantharaj et al. recommended normalizing the current response by FE and electrochemically active surface area (ECSA) to obtain a more accurate estimation of intrinsic catalytic activity.[45] We adopted this approach and used time-averaged partial current densities. Specifically, we corrected the TOF for the fraction of time spent at the cathodic potential via the duty cycle = $t_c/(t_a + t_c)$. We provide a detailed description of the TOF calculation in the Methods Section below. We corrected the exposed area by the roughness factor to accurately account for the density of

https://doi.org/10.1021/acscatal.3c04224
ACS Catal. 2024, 14, 785−796

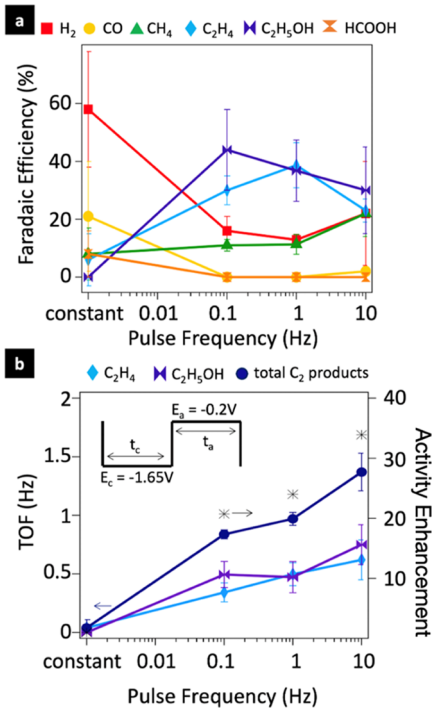

Figure 2. (a) Faradaic efficiency (%) of CO_2RR products as a function of the pulse frequency (Hz). (b) C_2 TOF (left axis) as a function of pulse frequency, where activity values are corrected for the electrode roughness factor and duty cycle. The ratio of enhancement (right axis) as a function of pulse frequency where enhancement ratio = C_2 TOF_{pulsed}/C_2 $TOF_{constant}$. Inset: Applied pulse profile: E_c = −1.65 $V_{Ag/AgCl}$, E_a = −0.2 $V_{Ag/AgCl}$, and $t_c = t_a$. Plotting average values from five measurements over 2 h ± one standard deviation from the mean. PF (s^{-1}) = $1/(t_a + t_c)$.

electrochemically active sites. This correction is especially important since the surface can change under cathodic conditions due to CO and H adsorption, and the presence of halides and pulsing can roughen the surface.[28,47−49] We estimated roughness factors based on double-layer capacitance measurements following electrolysis (see SI, Figure S3).

Pulsing the applied potential leads to a profound enhancement of C_2 activity, as evidenced by the TOF trends summarized in Figure 2b. Notably, pulsing increases the 2 h average C_2 TOF from ∼0.04 Hz in the potentiostatic reference case to ∼1 Hz and above for the pulsed potential CO_2 electrolysis. In the case of the 10 Hz PF, we observe a remarkable ∼33-fold enhancement in C_2 TOF compared to the potentiostatic case. The corresponding C_2 time-averaged, roughness factor corrected partial current density was ∼3.7 mA/cm_{ECSA}^2 (corresponding to an average instantaneous partial current density of ∼7.4 mA/cm_{ECSA}^2 during the cathodic step). We provide a full description of the product profile partial current densities in the SI (Figure S4). Beyond the internal comparison to our potentiostatic control experiments, we note the enhancement of the C_2 formation rate relative to comparable experiments reported in the literature (e.g., Hori et al. in 0.5 M KCl reported C_2 formation of ∼2 mA/cm_{geo}^2 at ∼−1.6 V vs Ag/AgCl and Kuhl et al. in 0.1 M $KHCO_3$ observed a C_2 formation of ∼1.8 mA/cm_{geo}^2 at ∼−1.75 V vs Ag/AgCl.[44,50]). Since we correct the activity data by the roughness factor, roughening does not explain the observed TOF enhancements. Moreover, we note that the enhancement in C_2 activity is considerably greater than the increase in CO_2 surface concentration due to the diffusion effects described above. Computational simulations of concentration gradients in the diffusive layer show that the CO_2 surface concentration is enhanced by only ∼50% compared to the constant potential scenario (see SI, Figure S1). Therefore, we can conclude that the pulse-enhanced C_2 activity is not due to concentration gradients in the diffusive layer but rather to changes in the EDL, as explained in the following sections.

The C_2 activity enhancement observed for fast pulse modulation (PF > TOF) warrants further discussion. Based on the premise that the sequence of electrochemical reactions involved in the transformation of CO_2 to C_2H_4 and C_2H_5OH must be completed within each respective cathodic pulse, we deduce that the PF defines the lower bound for the TOF. Accordingly, the actual C_2 TOF is likely appreciably larger than ∼1.3 Hz shown in Figure 2b. We interpret this comparison as an indication of the existence of highly active (i.e., TOF ≥ PF) surface active sites with an aerial density notably lower than that of Cu(100) top sites. The experimental trends in Figure 2b suggest that C_2 activity may be further enhanced with faster pulsing (PF > 10 Hz). Moreover, if PF defines the lower bound for TOF, pulsing the system at faster frequencies could, in principle, help to identify the maximum TOF for highly active sites. However, from a practical perspective, the range of experimentally accessible PFs is limited by the constraints of the potentiostat and the configuration of the electrochemical setup. Specifically, the rate of data collection and potentiostat buffer capacity currently limit multihour experiments at fast PF. The experimental trends in Figure 2b suggest that increasing PF beyond 10 Hz may enable further enhancements in the C_2 TOF. However, at high PF, the electrochemical system becomes limited by the RC charging time constant of the system (on the order of a few milliseconds), which will result in large losses to double-layer charging and decreased C_2 activity.[8]

To understand how competitive adsorption and reaction of *H and *CO impact the CO_2RR and HER, we devised a series of control experiments to disentangle the interplay between the two adsorbates. Our strategy combined control experiments focused solely on pulsed-electrolysis HER and analytical modeling. We examined the dynamics of hydrogen adsorption by measuring pulsed electrochemical HER in an Ar-saturated (i.e., CO_2-free) electrolyte. Like the reaction pathways for *CO (Figure 1c), the formation of H_2 can proceed via a dimerization- or insertion-type mechanism. In both pathways, the first step involves the formation of *H (i.e., the Volmer step), which can then either (i) couple with a proximate *H to form H_2 via the Volmer−Tafel pathway or (ii) react directly with a solvated proton via a concerted electrochemical path (i.e., Volmer−Heyrovsky mechanism).[51] The relative dominance of the two pathways depends on various factors, including the availability of protons (i.e., the pH in the EDL) and the applied overpotential. At the cathodic potentials tested (−1.65 V vs Ag/AgCl), we assume that there is minimal specific adsorption and that the adsorbates are noninteracting. Assuming the rate-determining step is H adsorption on top sites,[51,52] and that the rate of hydrogen absorption into the copper lattice is negligible,[53] HER current density can be used as a proxy for determining the amount of adsorbed hydrogen (*H) species.

In the pulsed electrochemical HER, the extent of hydrogen coverage on the electrode active sites is limited by the duration

https://doi.org/10.1021/acscatal.3c04224
ACS Catal. 2024, 14, 785−796

of the cathodic pulse. We examined the transient *H coverage by performing a series of HER control experiments at varying cathodic pulse durations. The experimental results in Figure 3

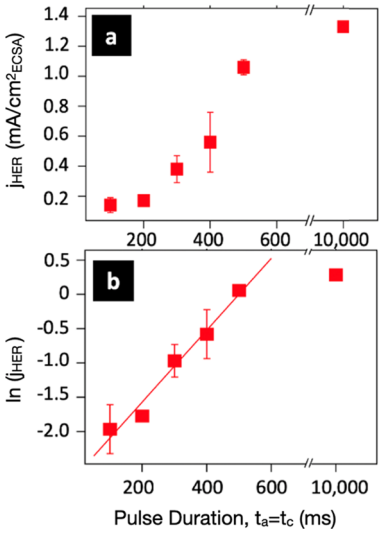

Figure 3. (a) Time-averaged roughness factor corrected partial current density of hydrogen formation as a function of pulse time. (b) Natural log of hydrogen partial current density as a function of pulse time. Pulse profile: E_c = −1.65 V, E_a = −0.2 V vs Ag/AgCl, and t_c = t_a in Ar-saturated 1 M KCl. Average between three measurements over 1 h ± one standard deviation.

show that the HER current density increases with extended cathodic pulse duration (i.e., decreasing PF). At long cathodic pulse durations ($t_c \gtrsim 500$ ms), the HER current density plateaus, which we interpret as the saturation coverage under the given electrolysis conditions. We analyzed the experimental data in the context of two analytical models to examine the (a) physical kinetics of the hydrated proton (i.e., hydronium ion, H_3O^+) diffusing through the boundary layer to the electrode surface and (b) the chemical kinetics associated with the adsorption of a proton on a catalyst surface site (*H). The analytical models (detailed in the SI) predict that in the case of diffusion-limited system, the HER partial current density should scale with the square root of the pulse duration (i.e., $J_{HER} \propto t_c^{1/2}$).[54,55] However, the diffusion-limited model does not adequately capture the experimental trends in the PF-dependent HER partial current density (see Figure S7). On the other hand, if the electron transfer rate is relatively slow, the transient *H coverage is kinetically limited, and the current density should scale with pulse time as $\ln(J_{HER}) \propto t$.[54,56] The PF-dependent HER partial current densities (Figure 3) are well-described by the kinetics limited model (Figure S8).

The observation that hydrogen adsorption is kinetically limited has several important repercussions on the transient HER current as well as the dynamic competition between *CO and *H for active sites on the copper electrode. Since the transient *H coverage is not limited by diffusive transport through the boundary layer (i.e., the availability of protons near the surface), the mechanistic interpretation here is independent of pH. The fact that the HER current density plateaus for cathodic pulse times longer than 500 ms suggests that pulsing at 1 Hz (t_c = t_a = 500 ms) or faster prevents *H from reaching its saturation coverage. The functional form of the HER current versus time (Figure 3a) is reminiscent of an adsorption isotherm in which fractional coverage increases with time from 0 monolayer (ML) coverage at short pulse times to a maximum, 1 ML coverage at >500 ms. To account for the fact that *H adsorption on Cu(100) first saturates hollow sites before adsorbing to top sites, we developed an analytical model to capture this adsorption sequence. Based on fits of this analytical model to the experimental data (SI, Figure S8), we can approximate the time required ($t' \approx 50$ ms) to saturate *H coverage on catalytically inactive hollow sites on Cu(100) surfaces before *H coverage is established on catalytically active Cu (100) top sites.

Translating insights into *H adsorption kinetics from the control experiment above to the scenario in which *H and *CO compete for surface sites requires consideration of several factors. Previous studies of the competing adsorption of *H and *CO showed that HER is inhibited in the presence of CO_2 and CO, suggesting that active sites for HER are covered with adsorbed CO.[57−59] We can, therefore, infer that the introduction of CO_2 and *CO extends the time required for hydrogen to reach a saturation coverage. We expanded the analytical model used to describe the HER control experiments to provide a more quantitative analysis of the dynamic competition of *CO and *H. This model involves two fitting parameters, ϕ and t', which incorporate the binding energy of the adsorbate and a delay time, respectively (see SI, Figure S9). We determined these parameters for the HER-only control experiments; however, similar control experiments to explicitly isolate the CO_2 reduction are experimentally not practical since HER cannot be eliminated in aqueous electrolytes. Instead, we systematically investigated a range of scenarios to examine how the ratio of ϕ and t' for the HER and CO_2RR impact the relative coverage of *CO and *H. This analysis suggests that the *CO/*H surface coverage ratio evolves nonlinearly as a function of time and, depending on the respective delay time and binding energy, can go through maxima at the early stages of the cathodic pulse. This interpretation is consistent with a recent report by Kim et al.,[35] who inferred that the *CO/*H ratio increases with decreasing pulse time based on the ratio of oxygenated/reduced reduction products detected with differential electrochemical mass spectroscopy.

The optimum *CO/*H ratio for C_2 products involves a delicate balance: too much *CO can block *H required for the hydrogenation steps, whereas too low *CO may impede C−C coupling. As far as we are aware, theoretical or computational models for the optimum *CO/*H ratio have not yet been established. The situation is likely complicated further by the experiment-specific interactions in the EDL (e.g., the composition and concentration of electrolytes). However, insights gleaned from pulsed CO_2RR experiments combined with basic analytical models highlight the significant potential and advantages of programming the pulse profile to modulate the temporal microenvironment and the ratio of *CO and *H coverage to enable future advances toward efficient C_2 production.

Binding Energies of *CO and *H from DFT. The dynamic competition between *CO and *H for surface sites is sensitive to the relative binding energies of the two adsorbates. To better understand the energetics associated with this competition, we turned to density functional theory (DFT) calculations. Our DFT calculations focused on *CO binding energies to Cu(100) as a function of competing *H coverage and applied potential. To ensure convergence of the binding energy, we carried out test calculations considering several factors, including the number of atomic layers, energy cutoff, *k*-

https://doi.org/10.1021/acscatal.3c04224
ACS Catal. 2024, 14, 785−796

point grid density, and vacuum spacing (see the SI). It is well established that hydrogen preferentially adsorbs on the face-centered cubic hollow sites of Cu(100), with the coverage being highly sensitive to the applied potential.[60,61] The detailed binding configuration of *CO on Cu(100) also requires careful consideration. We model *CO binding on top sites since $*CO_{atop}$ is most active toward C_2 products, whereas $*CO_{bridge}$ species have been identified as inactive for reduction.[42,45,58] Multiple studies have observed that $*CO_{atop}$ converts to $*CO_{bridge}$ over a relatively long time (i.e., minutes);[24,45] however, since our pulsing experiments are on the time scale of milliseconds, we assume all *CO is bound as $*CO_{atop}$. To determine the effect of hydrogen coverage on the binding energy of *CO, we examined three scenarios corresponding to zero, partial, and full *H coverage.

DFT calculations of the *CO binding energy to the top sites of a Cu (100) surface reveal several general trends (Figure 4). First, the *CO binding strength is essentially insensitive to the applied potential for a given *H coverage. This trend is consistent with previous computational studies reported in the literature.[57,60] Second, the *CO binding strength weakens significantly as the *H coverage in the hollow sites is increased from 0 to 1 ML; this trend is corroborated by the results previously published by Baricuatro et al.[60] Third, although the *CO binding energy is not directly affected by the applied potential, it is influenced by the fractional coverage of competing *H which itself is a function of potential. The *H fractional coverage (Θ_H) in the hollow sites increases with increasingly negative potentials.[53] As Θ_H in the hollow sites saturates, hydrogen binds to the top sites, where it competes with *CO for active sites[62] and can undergo H−H coupling for HER.[58]

The relative binding energies of *CO and *H revealed in the DFT calculations have interesting connections to theoretical microkinetic models recently examined by Baz et al.[32] Their analysis noted that changing the applied potential changes the free energy of the reaction for all steps equally, which is conceptually distinct from oscillating binding energies, which accelerates some steps at the expense of others. The combined insights from the theoretical model and computational simulations of binding energy hold particular significance for the mechanistic interpretation of the trends observed in our pulsed-electrolysis study. Although pulsing the applied potential does not induce oscillations in the binding energies of carbon-based species, it does lead to oscillations in the surface coverage of site-blocking *H, which, in turn, strengthens the *CO binding energy.

In combination, the relative binding energies of *CO and *H and the transient evolution of their surface coverage during the cathodic pulse offer important clues about the mechanism underlying the heightened C_2 activity enabled by pulsing electrolysis. During the anodic pulse, both CO and H are desorbed from the catalyst surface and replaced by concurrent adsorption of anions.[11,16,28] The buildup of *H coverage during the subsequent cathodic pulse is slower than *CO, which enhances the binding energy of CO compared to potentiostatic conditions and thereby creates a dynamic microenvironment for more efficient C−C coupling. In other words, the oscillation between anodic and cathodic potentials appears to create a modest positive feedback loop, thereby tilting the competition between H and CO in favor of the latter. This interpretation is corroborated by the CO activity trends (SI, Figure S19), which reveal a high TOF under constant potential conditions, whereas in the case of pulsed electrolysis, the CO partial current density is almost completely suppressed. Taken together, the DFT calculations of binding energies and the corresponding experiments show

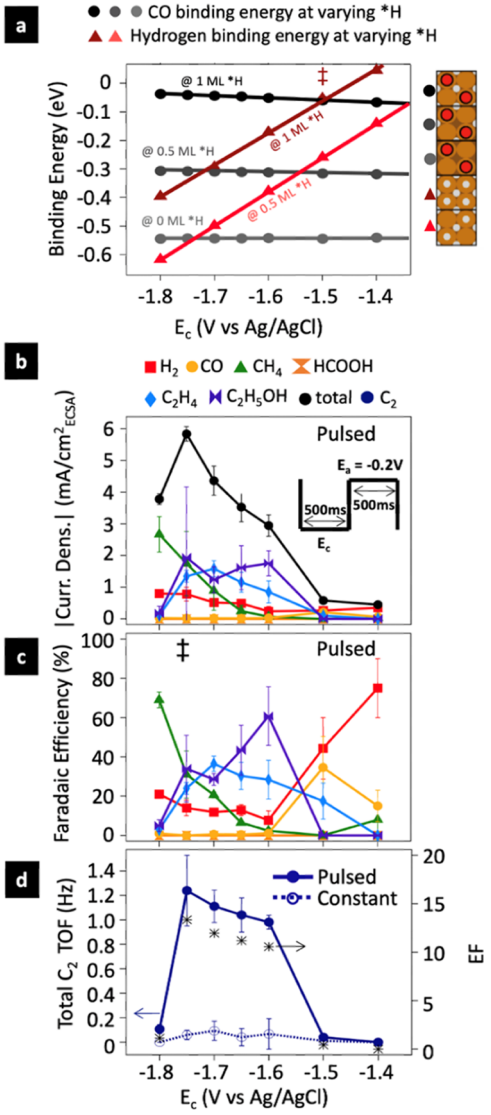

Figure 4. Comparison of DFT-calculated binding energy and experimental results. (a) DFT-calculated binding energies of top-bound CO as a function of the applied potential and *H coverage in the hollow sites (gray) and top-bound H as a function of the applied potential and coverage on the top sites (red). Lines are added to guide the reader's eye. For H binding energy data points, the *H coverage is 1 ML in the hollow sites. ‡ Indicates the crossover potential at which the hydrogen binding energy at 1 ML in the top sites shifts from positive (unfavorable) to negative (favorable), indicating that it becomes possible for *H to take over full coverage on the top sites at more negative potentials. Corresponding pulsed-electrolysis experimental trends as a function of the applied cathodic pulse potential in V vs Ag/AgCl: (b) reaction activity (current density, mA/cm_{ECSA}^2), (c) reaction selectivity (FE, %). ‡ Indicates the approximate crossover potential at which H binding becomes more favorable than CO binding, as indicated by the shift from C_2 products to CH_4. (d) TOF for C_2 products (ethylene + ethanol). Enhancement factor (EF = C_2 TOF_{pulsed}/C_2 $TOF_{constant\ at-1.7V}$). Pulse profile: E_c, E_a = −0.2 $V_{Ag/AgCl}$, $t_c = t_a$ = 500 ms. Plotting average values from five measurements over two h ± one standard deviation.

https://doi.org/10.1021/acscatal.3c04224
ACS Catal. 2024, 14, 785−796

that pulsing the applied potential effectively strengthens the *CO binding to enhance conversion to C_2 products.

We expect the trends of enhanced *CO binding and increased C_2 formation to be true whether pulsing desorbs *H from only the top sites or from both the top sites and hollow sites. Even if pulsing only reduces *H coverage on top sites, this frees top sites for *CO and increases the concentration of vacant sites, which reduces repulsive interactions among bound intermediates and strengthens the binding. A study by Zhang et al. using highly concentrated water-in-salt electrolytes found that while the rate-determining C−C coupling step is proton independent, reducing the activity of water increased C_2 production by decreasing the surface coverage of Cu−H and increasing available sites for *CO.[63] We suggest that pulsing the applied potential results in a similar effect. Under conditions of sufficiently high overpotentials, we expect the electrode surface to be completely covered with *H. In this case, other intermediates cannot adsorb,[61] and we would expect to observe only HER. Constant potential control experiments support this interpretation (SI, Figure S17). Conversely, pulsed electrolysis under increasingly negative potentials is not dominated by the HER, which indicates that pulsing effectively manages and suppresses the *H coverage (Figure 4).

The potential dependence of the relative binding energies of *H and *CO provides an interesting point of comparison between DFT calculations and experiments. The DFT calculations suggest that a "crossover" point is reached as the potential is made more negative, at which *H binding outcompetes *CO for top sites. An experimental signature of this crossover would be a significant decrease in C_2 production and a corresponding increase in hydrogen and/or C_1 products. Moreover, the DFT model predicts that pulsing reduces *H coverage and thereby extends the applied potential window for C_2 to higher (i.e., more negative) overpotentials. We put these predictions to the test by investigating the impact of increasingly negative cathodic pulse potentials on the C_2 activity.

Pulsed-electrolysis experiments with varying cathodic pulse potentials revealed increasing C_2 activity with an increasing potential up to a crossover point (‡ = −1.75 V). Beyond this point, C_2 formation drops significantly with a corresponding rise in CH_4 production. Given that HER is suppressed under all millisecond pulse conditions, we propose that the increased *H binding strength at more negative potentials reduces the site availability for *CO, thereby inhibiting C−C coupling and instead enhancing the formation of protonated C_1 products (i.e., CH_4). The exact value of the crossover potential from DFT cannot be interpreted quantitatively because the calculations assume idealized conditions and do not account for all experimental variations. However, the DFT results substantiate the existence of a crossover point where *H overtakes top site coverage, as the potential is made more negative. Figure 4a shows that *CO binding becomes weaker with increased hydrogen coverage but is insensitive to changes in potential, while *H binding becomes stronger at more negative potentials. This supports the idea that *H outcompetes *CO for top sites at more negative potentials, providing an explanation for the experimentally observed drop-off in C_2 production at −1.75 V. The correlation in potentials and qualitative trends between DFT and experiment highlights the importance and mutual advantages of integrating experiments and computations to formulate mechanistic models.

The combination of experiments and calculations allowed us to establish general design principles for the optimum pulse conditions to improve C_2 formation. Specifically, we identified the optimum window of cathodic pulse potentials (E_c range of −1.6 to −1.75 V) in which pulsing enhances the C_2 activity by a factor of ∼12 compared to the best-performing constant potential case (−1.7 V) We interpret this trend as an example of the dynamic catalysis case in the presence of competitive adsorbates previously discussed in theoretical models by Baz et al. Their model suggested that the highest activity enhancements occurred in cases with intermediate potentials that balance the effects of increased reaction speed for the desired pathway versus increased accumulation of site-blocking species with the increasing overpotential.[32]

We hypothesize that not only are we increasing the coverage of *CO under pulsed conditions, but we are also pulsing at time scales that affect the coverage of site-blocking *H species, which changes the binding characteristics of *CO to have more available sites and stronger binding. We show the critical role of controlling the dynamic competition of *CO and *H, and the novelty of our approach is derived from the dynamic modulation of the surface coverages by controlling the potential and duration.

CONCLUSIONS

Achieving high reaction activity toward C_2 products requires a balance between adsorbed *CO and *H. The experiments and computational models presented in this study show that pulsing the applied potential provides a simple and versatile approach to investigating and moderating this balance. As a compelling example of the benefits of dynamic electrocatalysis, our experiments showed that pulsing the applied potential enhances the electrocatalytic activity of C−C coupling (i.e., C_2 TOF) by as much as 33-fold compared to potentiostatic electrolysis. We interpret this enhanced activity in the context of oscillating surface coverage and the transient nature of *CO/*H coverage during the cathodic pulse. We established the oscillating binding energies impact the dynamic competition between *CO and *H for available surface sites and how these trends explain the observed frequency and potential dependent product selectivity trends. Increasing pulse frequency leads to increasing C_2 activity because shorter cathodic pulse times prevent *H from reaching saturation coverage. This reduced *H coverage frees up more sites for CO_2RR intermediates as well as strengthens the binding strength of CO. Combining theory with experiments elucidates more information on the effects of HER suppression in the pulsing mechanism in the context of dynamic catalysis, explaining why pulsing extends the window of C_2 activity by shifting the crossover potential (where *H becomes more favorable than *CO) more negative. Looking ahead, this work paves the way for exciting opportunities to harness both spatial and temporal modifications of the microenvironment to customize the synthesis toward specific products. The significant impact of this research lies in offering a more profound mechanistic understanding of pulsed electrolysis, as well as providing design principles to drive future advances in programmable CO_2 reduction with optimized activity, selectivity, and durability for the creation of high-value products.

https://doi.org/10.1021/acscatal.3c04224
ACS Catal. 2024, 14, 785−796

METHODS

Electrode Fabrication and Electrolyte Preparation. The working electrode was a polycrystalline copper foil (Puratronic, 99.9999% Alfa Aesar) connected to a titanium wire (Aldrich) with silver paint (Leitsilber 200, Ted Pella Inc.). The back and edges were then covered with an inert epoxy (Omegabond 101), leaving an exposed geometric surface area of ∼0.2 cm^2. Prior to use in the cell, the electrode was electropolished in 85% phosphoric acid (Macron Fine Chemicals) to remove any impurities and surface oxides, leaving a mirror finish. After electropolishing, the electrode was thoroughly rinsed with DI water and immediately put into the cell.

The 1 M electrolyte was prepared with KCl (Sigma-Aldrich, ACS Reagent 99.0−100.5%) and 18.2 MΩ DI water (ELGA LabWater) and then stirred with Chelex resin (Chelex100, sodium form, Sigma-Aldrich) for at least 24 h prior to usage.[64,65] CO_2-saturated KCl has a pH of ∼3.8.[12]

Electrochemical Measurements and Product Characterization. The cell used was a custom-made two-compartment glass H-cell with a Cu foil working electrode, a Ag/AgCl reference electrode (Pine Instruments), a platinum mesh counter electrode (99.9999%, Alfa Aesar), and a Nafion 117 cation exchange membrane separating the anode and cathode compartments. Potentials were applied, and 85% *iR* was compensated in situ using a Biologic SP-300 potentiostat. All experiments were conducted at room temperature. The electrolyte was saturated with CO_2 (Research 5.0 grade, Airgas) for at least 30 min prior to applying a potential, and during the experiments, CO_2 was bubbled through at a controlled rate of 1.4 sccm using a mass flow controller (Bronkhorst EL-FLOW Select series). The cell outlet was connected directly to a GC (SRI, Multigas #5) equipped with FID and TCD detectors. Argon (Airgas) was used as a carrier gas, and hydrogen from a hydrogen generator (H2−100, SRI Instruments) was used for the FID. Liquid aliquots were taken at the end for ^1H NMR analysis (Bruker AV-500). The NMR samples were prepared by mixing an aliquot of the electrolyte after measurement with D_2O (99.9 atom % D, Aldrich) and 500 μM dimethyl sulfoxide (Fisher Chemical) solution in a 1:1:8 volume ratio.

Product characterization took place beginning 10 min into electrolysis and every 24 min thereafter (16 min run and 8 min cooldown time). The Coulombs needed to produce that concentration of each product were calculated and divided by the total coulombs put into the system to determine the Faradaic efficiency. The total Coulomb input to the system was determined by extracting the Faradaic cathodic current from the chronoamperometry data and correcting for the duty cycle as explained in previous works.[11] Partial current density for a given product was calculated by multiplying the time-averaged total current density by the corresponding product current efficiency.

TOF Calculation. The turnover frequency (TOF) represents the number of turnovers of a catalytic cycle with respect to time per active site and can be calculated as follows[45]

$$\mathrm{TOF}_x\ (\mathrm{s}^{-1}) = \frac{j_x\ (\mathrm{mA/cm^2}) \times N_A\ (\mathrm{atoms/mol})}{F\ (\mathrm{C/mol\ e^-}) \times n_x\ (\mathrm{mol\ e^-/mol}\ x) \times \Gamma\ (\mathrm{sites/\ cm^2})}$$

where j_x (mA/cm^2) is the duty cycle corrected time-averaged partial current density of product *x*, *A* (cm^2) is the electrode area, N_A (atoms/mol) is Avogadro's number, *F* (C/mol e^-) is Faraday's constant, n_x (mol e^-/mol *x*) is the moles of electrons needed to generate one mole of product, and Γ (sites/cm^2) is the surface density of active sites available assuming each Cu top atom on the Cu(100) surface presents one active site.

Copper is arranged in a face-centered cubic configuration. We assume each exposed surface atom is an active site, and we also correct the number of sites available by the roughness factor, which we estimate with double-layer capacitance measurements.

There are two atoms (= two active sites) per a^2, or 1.54 × 10^{15} surface atoms/cm^2.[66] To get the number of surface atoms available in a given experiment, we multiply the number of surface atoms/cm^2 by the electrochemically active surface area of the electrode ($A_{ECSA} = A_{geo} \times RF$), where A_{geo} is the geometric electrode area and RF is the roughness factor.

We note that there is likely to be some error in our calculation due to variability in the C_{dl} measurements and that there are variations in crystallographic data, especially on the polycrystalline material.[45]

DFT Methods. The binding energy relates the energy of the molecule adsorbed on the surface to the energy of the clean surface and desorbed molecule. Carbon monoxide binding energies on Cu(100) were calculated at 0.5 ML using a $\sqrt{2} \times \sqrt{2}$ supercell with two copper atoms per layer. The 0.5 ML coverage was modeled based on work from Baricuatro et al. that showed that *CO coverage equilibrates at 0.5 ML at potentials favorable for *CO adsorption and in agreement with other studies suggesting a maximum CO coverage of 0.44 ML on the on top sites.[47,60,67]

The binding energy of *CO on Cu(100) can be defined as follows[68]

$$E_b = \frac{1}{n}(E_{*\mathrm{COonCu100}} - (E_{\mathrm{Cu100}} + nE_{\mathrm{CO}})) \quad (1)$$

where *n* is the number of molecules adsorbed on the slab and $E_{*COonCu100}$, E_{Cu100}, and E_{CO} are the DFT-calculated total energies of the *CO molecule(s) on the slab, the clean slab, and the free CO molecule, respectively.

DFT calculations were carried out within the plane-wave basis software JDFTx using the generalized gradient approx-

https://doi.org/10.1021/acscatal.3c04224
ACS Catal. 2024, 14, 785−796

imation (GGA).[69−71] All calculations employed ultrasoft Perdew−Burke−Ernzerhof (PBE) pseudopotentials from the GBRV pseudopotential library.[72] The revised PBE exchange functional (as modified by Hammer et al.) was used because it was specifically developed to improve *CO binding energy predictions and has been shown to predict *CO binding energies and preferred adsorption sites in better agreement with the experiment.[73−75] For example, Gameel et al. show that the RPBE exchange functional correctly predicts the adsorption site of *CO on Cu(100), as compared to the PW91 functional, which incorrectly predicts that *CO prefers adsorption on the bridge site over the top site.[76] These results were independently verified, and the DFT-calculated binding energies were found to be in good agreement with the values reported in their paper and with the experimental binding energy reported by Vollmer et al.[77] We excluded van der Waals corrections to the DFT calculations based on the work of Janthon et al., who compared experimental CO/Pt(111) binding energies measured through microcalorimetry to DFT calculations using eight different functionals with and without dispersion corrections. Based on their work, the RPBE and RevPBE functionals without van der Waals corrections did not improve the site preference but showed the closest agreement with the experimentally determined values.[78]

Lattice optimization of bulk copper was performed in JDFTx, and the resulting lattice parameter was 3.79 Å, in good agreement with the experimental value of 3.61 Å.[79] The atomic simulation environment (ASE) was used to set up the geometries of the copper slabs at the computationally determined lattice parameter.[80]

Test calculations were carried out to converge the binding energy with respect to the number of atomic layers, energy cutoff, k-point grid density, and vacuum spacing (Supporting Figures). We used a four-layer slab with the bottom two atomic layers fixed, while the top two layers and the adsorbates were allowed to relax to the minimum energy positions. For calculations involving metal slabs, we used the Fermi electron smearing at a width of 0.01 Ha to aid convergence. An energy cutoff of 15 Ha with a charge density cutoff of 60 Ha, Monkhorst−Pack k-point grid sampling of 4 × 4 × 1, and vacuum spacing of 10 Å was found to be sufficient to converge the binding energy to <20 meV, which is well within the limits of DFT accuracy. The total energy of the CO molecule was calculated using the same energy cutoff in a cubic box of side length 20 Bohr. Due to the high computational expense of modeling explicit solvent molecules, the solvent was modeled implicitly using the NonlinearPCM fluid model.[81] Electrostatic nonadsorbing ions were included at a concentration of 1.0 M.

For calculations involving metal slabs, the applied potential was varied using the grand-canonical feature of JDFTx,[82] which allows the number of electrons to equilibrate to the specified electron chemical potential and corrects the resulting Helmholtz free energy to the grand free energy. For reference to the isolated CO molecule, the total energy of the CO molecule was calculated at the neutral potential (fixed number of electrons), and the energy was shifted by $-n\mu$, where n is the total number of valence electrons in the pseudopotential DFT calculation and μ is the electron chemical potential, equivalent to $\mu_{SHE}-U$, where μ_{SHE} is the absolute SHE potential (set to 4.44 V based on experiment) and U is the applied potential.[82] Further details about the JDFTx fixed potential calculations are included in the SI.

■ ASSOCIATED CONTENT

Supporting Information

The Supporting Information is available free of charge at https://pubs.acs.org/doi/10.1021/acscatal.3c04224.

Calculated spatiotemporal CO_2 gradients near the electrode surface; electrode structure characterization (XRD); electrochemically active surface area estimation from double-layer capacitance; full product profile and partial current density measurements; HER-only control experiments; and analytical model for dynamic competitive adsorption (PDF)

■ AUTHOR INFORMATION

Corresponding Author

Tobias Hanrath − *Robert F. Smith School of Chemical and Biomolecular Engineering, Cornell University, Ithaca, New York 14853, United States;* orcid.org/0000-0001-5782-4666; Email: tobias.hanrath@cornell.edu

Authors

Rileigh Casebolt DiDomenico − *Robert F. Smith School of Chemical and Biomolecular Engineering, Cornell University, Ithaca, New York 14853, United States;* orcid.org/0000-0002-1134-1666

Kelsey Levine − *Robert F. Smith School of Chemical and Biomolecular Engineering, Cornell University, Ithaca, New York 14853, United States*

Colin Bundschu − *Department of Physics, Cornell University, Ithaca, New York 14853, United States*

Laila Reimanis − *Department of Physics, Cornell University, Ithaca, New York 14853, United States;* orcid.org/0000-0002-9341-5015

Tomas Arias − *Department of Physics, Cornell University, Ithaca, New York 14853, United States*

Complete contact information is available at: https://pubs.acs.org/10.1021/acscatal.3c04224

Author Contributions

[§]R.C.D. and K.L. contributed equally to this work. The manuscript was written through contributions of all authors. All authors have given approval to the final version of the manuscript.

Funding

This work was supported in part by the National Science Foundation (NSF) CBET1805400. R.C.D. was supported by the CESI-Corning Graduate Fellowship. K.L. and L.R. acknowledge support from the Cornell Engineering Learning Initiative. This work made use of the Cornell University NMR Facility, which is supported, in part, by the NSF through MRI award CHE-1531632.

Notes

The authors declare no competing financial interest.

■ ACKNOWLEDGMENTS

This work was supported in part by the National Science Foundation (NSF) CBET1805400. R.C.D. was supported by the CESI-Corning Graduate Fellowship. K.L. and L.R. acknowledge support from the Cornell Engineering Learning Initiative. This work made use of the Cornell University NMR Facility, which is supported, in part, by the NSF through MRI award CHE-1531632. This research was also conducted with

support from the Cornell University Center for Advanced Computing, which receives funding from Cornell University, the National Science Foundation, and members of its Partner Program. We would additionally like to thank Ravishankar Sundararaman and Nicole A. Benedek for their help in setting up the DFT calculations and Prof. Hector Abruña discussions on adsorption models.

■ ABBREVIATIONS

TOF –turnover frequency; CO_2RR –CO_2 reduction reaction; PF –pulse frequency; ECSA –electrochemically active surface area

■ REFERENCES

(1) De Luna, P.; Hahn, C.; Higgins, D.; Jaffer, S. A.; Jaramillo, T. F.; Sargent, E. H. What would it take for renewably powered electrosynthesis to displace petrochemical processes? *Science* **2019**, *364* (6438), No. eaav3506.
(2) Nitopi, S.; Bertheussen, E.; Scott, S. B.; Liu, X.; Engstfeld, A. K.; Horch, S.; Seger, B.; Stephens, I. E.; Chan, K.; Hahn, C.; Nørskov, J. K.; Jaramillo, T. F.; Chorkendorff, I. Progress and perspectives of electrochemical CO2 reduction on copper in aqueous electrolyte. *Chem. Rev.* **2019**, *119* (12), 7610−7672.
(3) Bagger, A.; Ju, W.; Varela, A. S.; Strasser, P.; Rossmeisl, J. Electrochemical CO2 reduction: a classification problem. *ChemPhysChem* **2017**, *18* (22), 3266−3273.
(4) Xiang, K.; Shen, F.; Fu, Y.; Wu, L.; Wang, Z.; Yi, H.; Liu, X.; Wang, P.; Liu, M.; Lin, Z.; Liu, H. Boosting CO2 electroreduction towards C2+ products via CO* intermediate manipulation on copper-based catalysts. *Environ. Sci.: Nano* **2022**, *9* (3), 911−953.
(5) Shao, F.; Wong, J. K.; Low, Q. H.; Iannuzzi, M.; Li, J.; Lan, J. In situ spectroelectrochemical probing of CO redox landscape on copper single-crystal surfaces. *Proc. Natl. Acad. Sci. U.S.A.* **2022**, *119* (29), No. e2118166119.
(6) Vassalini, I.; Alessandri, I. Switchable Stimuli-Responsive Heterogeneous Catalysis. *Catalysts* **2018**, *8* (12), No. 569, DOI: 10.3390/catal8120569.
(7) Ardagh, M. A.; Abdelrahman, O. A.; Dauenhauer, P. J. Principles of Dynamic Heterogeneous Catalysis: Surface Resonance and Turnover Frequency Response. *ACS Catal.* **2019**, *9* (8), 6929−6937.
(8) Casebolt, R.; Levine, K.; Suntivich, J.; Hanrath, T. Pulse check: Potential opportunities in pulsed electrochemical CO2 reduction. *Joule* **2021**, *5* (8), 1987−2026.
(9) Kim, C.; Weng, L.-C.; Bell, A. T. Impact of pulsed electrochemical reduction of CO2 on the formation of C2+ products over Cu. *ACS Catal.* **2020**, *10* (21), 12403−12413.
(10) Wasmus, S.; Cattaneo, E.; Vielstich, W. Reduction of carbon dioxide to methane and ethene—an on-line MS study with rotating electrodes. *Electrochim. Acta* **1990**, *35* (4), 771−775.
(11) Kimura, K. W.; Fritz, K. E.; Kim, J.; Suntivich, J.; Abruña, H. D.; Hanrath, T. Controlled selectivity of CO2 reduction on copper by pulsing the electrochemical potential. *ChemSusChem* **2018**, *11* (11), 1781−1786.
(12) Casebolt, R.; Kimura, K. W.; Levine, K.; DaSilva, J. A. C.; Kim, J.; Dunbar, T. A.; Suntivich, J.; Hanrath, T. Effect of electrolyte composition and concentration on pulsed potential electrochemical CO2 reduction. *ChemElectroChem* **2021**, *8* (4), 681−688, DOI: 10.1002/celc.202001445.
(13) Shiratsuchi, R.; Aikoh, Y.; Nogami, G. Pulsed electroreduction of CO 2 on copper electrodes. *J. Electrochem. Soc.* **1993**, *140* (12), No. 3479, DOI: 10.1149/1.2221113.
(14) Friebe, P.; Bogdanoff, P.; Alonso-Vante, N.; Tributsch, H. A real-time mass spectroscopy study of the (electro) chemical factors affecting CO2 reduction at copper. *J. Catal.* **1997**, *168* (2), 374−385.
(15) Jännsch, Y.; Leung, J. J.; Hämmerle, M.; Magori, E.; Wiesner-Fleischer, K.; Simon, E.; Fleischer, M.; Moos, R. Pulsed potential electrochemical CO2 reduction for enhanced stability and catalyst reactivation of copper electrodes. *Electrochem. Commun.* **2020**, *121*, No. 106861.
(16) Duff, C. S. L.; Lawrence, M. J.; Rodriguez, P. Role of the adsorbed oxygen species in the selective electrochemical reduction of CO2 to alcohols and carbonyls on copper electrodes. *Angew. Chem.* **2017**, *129* (42), 13099−13104, DOI: 10.1002/ange.201706463.
(17) Arán-Ais, R. M.; Scholten, F.; Kunze, S.; Rizo, R.; Roldan Cuenya, B. The role of in situ generated morphological motifs and Cu(I) species in C2+ product selectivity during CO2 pulsed electroreduction. *Nat. Energy* **2020**, *5* (4), 317−325.
(18) Engelbrecht, A.; Uhlig, C.; Stark, O.; Hämmerle, M.; Schmid, G.; Magori, E.; Wiesner-Fleischer, K.; Fleischer, M.; Moos, R. On the electrochemical CO2 reduction at copper sheet electrodes with enhanced long-term stability by pulsed electrolysis. *J. Electrochem. Soc.* **2018**, *165* (15), No. J3059, DOI: 10.1149/2.0091815jes.
(19) Bui, J. C.; Kim, C.; Weber, A. Z.; Bell, A. T. Dynamic boundary layer simulation of pulsed CO2 electrolysis on a copper catalyst. *ACS Energy Lett.* **2021**, *6* (4), 1181−1188.
(20) Kim, C.; Bui, J. C.; Luo, X.; Cooper, J. K.; Kusoglu, A.; Weber, A. Z.; Bell, A. T. Tailored catalyst microenvironments for CO2 electroreduction to multicarbon products on copper using bilayer ionomer coatings. *Nat. Energy* **2021**, *6* (11), 1026−1034.
(21) Nogami, G.; Itagaki, H.; Shiratsuchi, R. Pulsed Electroreduction of CO2 on Copper Electrodes-II. *J. Electrochem. Soc.* **1994**, *141* (5), No. 1138, DOI: 10.1149/1.2054886.
(22) Jermann, B.; Augustynski, J. Long-term activation of the copper cathode in the course of CO2 reduction. *Electrochim. Acta* **1994**, *39* (11−12), 1891−1896.
(23) Lim, C.; Harrington, D.; Marshall, A. Altering the selectivity of galvanostatic CO2 reduction on Cu cathodes by periodic cyclic voltammetry and potentiostatic steps. *Electrochim. Acta* **2016**, *222*, 133−140.
(24) Lin, S.-C.; Chang, C.-C.; Chiu, S.-Y.; Pai, H.-T.; Liao, T.-Y.; Hsu, C.-S.; Chiang, W.-H.; Tsai, M.-K.; Chen, H. M. Operando time-resolved X-ray absorption spectroscopy reveals the chemical nature enabling highly selective CO2 reduction. *Nat. Commun.* **2020**, *11* (1), No. 3525, DOI: 10.1038/s41467-020-17231-3.
(25) Kimura, K. W.; Casebolt, R.; DaSilva, J. C.; Kauffman, E.; Kim, J.; Dunbar, T. A.; Pollock, C. J.; Suntivich, J.; Hanrath, T. Selective electrochemical CO2 reduction during pulsed potential stems from dynamic interface. *ACS Catal.* **2020**, *10* (15), 8632−8639, DOI: 10.1021/acscatal.0c02630.
(26) Tang, Z.; Nishiwaki, E.; Fritz, K. E.; Hanrath, T.; Suntivich, J. Cu(I) reducibility controls ethylene vs ethanol selectivity on (100)-textured copper during pulsed CO2 reduction. *ACS Appl. Mater. Interfaces* **2021**, *13* (12), 14050−14055.
(27) Strain, J. M.; Gulati, S.; Pishgar, S.; Spurgeon, J. M. Pulsed Electrochemical Carbon Monoxide Reduction on Oxide-Derived Copper Catalyst. *ChemSusChem* **2020**, *13* (11), 3028−3033.
(28) DiDomenico, R. C.; Hanrath, T. Pulse Symmetry Impacts the C2 Product Selectivity in Pulsed Electrochemical CO2 Reduction. *ACS Energy Lett.* **2022**, *7*, 292−299.
(29) Kumar, B.; Brian, J. P.; Atla, V.; Kumari, S.; Bertram, K. A.; White, R. T.; Spurgeon, J. M. Controlling the product syngas H2: CO ratio through pulsed-bias electrochemical reduction of CO2 on copper. *ACS Catal.* **2016**, *6* (7), 4739−4745.
(30) Ardagh, M. A.; Abdelrahman, O. A.; Dauenhauer, P. J. Principles of dynamic heterogeneous catalysis: surface resonance and turnover frequency response. *ACS Catal.* **2019**, *9* (8), 6929−6937.
(31) Gopeesingh, J.; Ardagh, M. A.; Shetty, M.; Burke, S. T.; Dauenhauer, P. J.; Abdelrahman, O. A. Resonance-promoted formic acid oxidation via dynamic electrocatalytic modulation. *ACS Catal.* **2020**, *10* (17), 9932−9942.
(32) Baz, A.; Lyons, M.; Holewinski, A. Dynamic Electrocatalysis: Examining Resonant Catalytic Rate Enhancement Under Oscillating Electrochemical Potential. *Chem. Catal.* **2022**, *2*, 3497−3516, DOI: 10.1016/j.checat.2022.09.002.
(33) Timoshenko, J.; Bergmann, A.; Rettenmaier, C.; Herzog, A.; Arán-Ais, R. M.; Jeon, H. S.; Haase, F. T.; Hejral, U.; Grosse, P.; Kühl,

S.; et al. Steering the structure and selectivity of CO2 electroreduction catalysts by potential pulses. *Nat. Catal.* **2022**, *5*, 259−267.
(34) Engelbrecht, A.; Uhlig, C.; Stark, O.; Hämmerle, M.; Schmid, G.; Magori, E.; Wiesner-Fleischer, K.; Fleischer, M.; Moos, R. On the Electrochemical CO2Reduction at Copper Sheet Electrodes with Enhanced Long-Term Stability by Pulsed Electrolysis. *J. Electrochem. Soc.* **2018**, *165* (15), J3059−J3068.
(35) Kim, C.; Weng, L. C.; Bell, A. T. Impact of Pulsed Electrochemical Reduction of CO2 on the Formation of C2+ Products over Cu. *ACS Catal.* **2020**, *10* (21), 12403−12413.
(36) Resasco, J.; Abild-Pedersen, F.; Hahn, C.; Bao, Z.; Koper, M.; Jaramillo, T. F. Enhancing the connection between computation and experiments in electrocatalysis. *Nat. Catal.* **2022**, *5* (5), 374−381.
(37) Shin, S.-J.; Kim, D. H.; Bae, G.; Ringe, S.; Choi, H.; Lim, H.-K.; Choi, C. H.; Kim, H. On the importance of the electric double layer structure in aqueous electrocatalysis. *Nat. Commun.* **2022**, *13* (1), No. 174, DOI: 10.1038/s41467-021-27909-x.
(38) Ringe, S.; Morales-Guio, C. G.; Chen, L. D.; Fields, M.; Jaramillo, T. F.; Hahn, C.; Chan, K. Double layer charging driven carbon dioxide adsorption limits the rate of electrochemical carbon dioxide reduction on Gold. *Nat. Commun.* **2020**, *11* (1), No. 33, DOI: 10.1038/s41467-019-13777-z.
(39) Pan, B.; Wang, Y.; Li, Y. Understanding and leveraging the effect of cations in the electrical double layer for electrochemical CO2 reduction. *Chem. Catal.* **2022**, *2* (6), 1267−1276.
(40) Resasco, J.; Chen, L. D.; Clark, E.; Tsai, C.; Hahn, C.; Jaramillo, T. F.; Chan, K.; Bell, A. T. Promoter Effects of Alkali Metal Cations on the Electrochemical Reduction of Carbon Dioxide. *J. Am. Chem. Soc.* **2017**, *139* (32), 11277−11287.
(41) Zhi, X.; Vasileff, A.; Zheng, Y.; Jiao, Y.; Qiao, S.-Z. Role of oxygen-bound reaction intermediates in selective electrochemical CO 2 reduction. *Energy Environ. Sci.* **2021**, *14* (7), 3912−3930.
(42) Dinh, C.-T.; Burdyny, T.; Kibria, M. G.; Seifitokaldani, A.; Gabardo, C. M.; de Arquer, F. P. G.; Kiani, A.; Edwards, J. P.; De Luna, P.; Bushuyev, O. S.; et al. CO2 electroreduction to ethylene via hydroxide-mediated copper catalysis at an abrupt interface. *Science* **2018**, *360* (6390), 783−787, DOI: 10.1126/science.aas9100.
(43) He, M.; Li, C.; Zhang, H.; Chang, X.; Chen, J. G.; Goddard, W. A.; Cheng, M.-J.; Xu, B.; Lu, Q. Oxygen induced promotion of electrochemical reduction of CO2 via co-electrolysis. *Nat. Commun.* **2020**, *11* (1), No. 3844, DOI: 10.1038/s41467-020-17690-8.
(44) Hori, Y.; Murata, A.; Takahashi, R. Formation of hydrocarbons in the electrochemical reduction of carbon dioxide at a copper electrode in aqueous solution. *J. Chem. Soc., Faraday Trans. 1* **1989**, *85* (8), 2309−2326, DOI: 10.1039/f19898502309.
(45) Anantharaj, S.; Karthik, P. E.; Noda, S. The significance of properly reporting turnover frequency in electrocatalysis research. *Angew. Chem., Int. Ed.* **2021**, *60* (43), 23051−23067.
(46) Chan, K. A few basic concepts in electrochemical carbon dioxide reduction. *Nat. Commun.* **2020**, *11* (1), No. 5954, DOI: 10.1038/s41467-020-19369-6.
(47) Roiaz, M.; Falivene, L.; Rameshan, C.; Cavallo, L.; Kozlov, S. M.; Rupprechter, G. Roughening of copper (100) at elevated CO pressure: Cu adatom and cluster formation enable CO dissociation. *J. Phys. Chem. C* **2019**, *123* (13), 8112−8121, DOI: 10.1021/acs.jpcc.8b07668.
(48) Matsushima, H.; Taranovskyy, A.; Haak, C.; Gründer, Y.; Magnussen, O. M. Reconstruction of Cu (100) electrode surfaces during hydrogen evolution. *J. Am. Chem. Soc.* **2009**, *131* (30), 10362−10363.
(49) Kwon, Y.; Lum, Y.; Clark, E. L.; Ager, J. W.; Bell, A. T. CO2 electroreduction with enhanced ethylene and ethanol selectivity by nanostructuring polycrystalline copper. *ChemElectroChem* **2016**, *3* (6), 1012−1019.
(50) Kuhl, K. P.; Cave, E. R.; Abram, D. N.; Jaramillo, T. F. New insights into the electrochemical reduction of carbon dioxide on metallic copper surfaces. *Energy Environ. Sci.* **2012**, *5* (5), 7050−7059.
(51) Sharifi-Asl, S.; Macdonald, D. D. Investigation of the kinetics and mechanism of the hydrogen evolution reaction on copper. *J. Electrochem. Soc.* **2013**, *160* (6), No. H382, DOI: 10.1149/2.143306jes.
(52) Bockris, J. O.; Pentland, N. The mechanism of hydrogen evolution at copper cathodes in aqueous solutions. *Trans. Faraday Soc.* **1952**, *48*, 833−839.
(53) Abd Elhamid, M. H.; Ateya, B.; Weil, K.; Pickering, H. Calculation of the hydrogen surface coverage and rate constants of the hydrogen evolution reaction from polarization data. *J. Electrochem. Soc.* **2000**, *147* (6), No. 2148, DOI: 10.1149/1.1393500.
(54) Tirado, J. D.; Acevedo, D.; Bretz, R. L.; Abruna, H. D. Adsorption dynamics of electroactive self-assembling molecules. *Langmuir* **1994**, *10* (6), 1971−1979.
(55) Reinmuth, W. H. Diffusion to a plane with Langmuirian adsorption. *J. Phys. Chem. A* **1961**, *65* (3), 473−476.
(56) Parsons, R. The Structure of the Electrical Double Layer and Its Influence on the Rates of Electrode Reactions. In *Advances Electrochemistry and Electrochemical Engineering*; Delahay, P., Ed.; Interscience Publishers, Inc., 1961; Vol. *1*, pp 1−64.
(57) Cheng, T.; Xiao, H.; Goddard, W. A., III Full atomistic reaction mechanism with kinetics for CO reduction on Cu(100) from ab initio molecular dynamics free-energy calculations at 298 K. *Proc. Natl. Acad. Sci. U.S.A.* **2017**, *114* (8), 1795−1800.
(58) Koga, O.; Teruya, S.; Matsuda, K.; Minami, M.; Hoshi, N.; Hori, Y. Infrared spectroscopic and voltammetric study of adsorbed CO on stepped surfaces of copper monocrystalline electrodes. *Electrochim. Acta* **2005**, *50* (12), 2475−2485.
(59) Shaw, S. K.; Berná, A.; Feliu, J. M.; Nichols, R. J.; Jacob, T.; Schiffrin, D. J. Role of axially coordinated surface sites for electrochemically controlled carbon monoxide adsorption on single crystal copper electrodes. *Phys. Chem. Chem. Phys.* **2011**, *13* (12), 5242−5251.
(60) Baricuatro, J. H.; Kwon, S.; Kim, Y.-G.; Cummins, K. D.; Naserifar, S.; Goddard, W. A., III Operando Electrochemical Spectroscopy for CO on Cu(100) at pH 1 to 13: Validation of Grand Canonical Potential Predictions. *ACS Catal.* **2021**, *11* (5), 3173−3181.
(61) Hussain, J.; Jónsson, H.; Skúlason, E. Calculations of product selectivity in electrochemical CO2 reduction. *ACS Catal.* **2018**, *8* (6), 5240−5249.
(62) Salimon, J.; Hernández-Romero, R.; Kalaji, M. The dynamics of the conversion of linear to bridge bonded CO on Cu. *J. Electroanal. Chem.* **2002**, *538-539*, 99−108.
(63) Zhang, H.; Gao, J.; Hall, A. S. Promoting Cu Catalyzed CO2 electroreduction to multi-carbon products by tuning the activity of water *ChemRxiv* 2022.
(64) Jovanov, Z. P.; de Araujo, J. F.; Li, S.; Strasser, P. Catalyst preoxidation and EDTA electrolyte additive remedy activity and selectivity declines during electrochemical CO2 reduction. *J. Phys. Chem. C* **2019**, *123* (4), 2165−2174, DOI: 10.1021/acs.jpcc.8b08794.
(65) Wuttig, A.; Surendranath, Y. Impurity ion complexation enhances carbon dioxide reduction catalysis. *ACS Catal.* **2015**, *5* (7), 4479−4484.
(66) Koroteev, Y. M.; Chulkov, E. V. Electronic and Crystal Structure of the Pt (111)-(2× 2)-K and Cu (111)-(2× 2)-K Systems. In *Advances in Quantum Chemistry*; Elsevier, 2019; Vol. *80*, pp 175−197.
(67) Wuttig, A.; Ryu, J.; Surendranath, Y. Electrolyte Competition Controls Surface Binding of CO Intermediates to CO2 Reduction Catalysts *ChemRxiv* 2019.
(68) Suleiman, I. A.; Radny, M. W.; Gladys, M. J.; Smith, P. V.; Mackie, J. C.; Kennedy, E. M.; Dlugogorski, B. Z. Interaction of chlorine and oxygen with the Cu (100) surface. *J. Phys. Chem. C* **2010**, *114* (44), 19048−19054.
(69) Freysoldt, C.; Boeck, S.; Neugebauer, J. Direct minimization technique for metals in density functional theory. *Phys. Rev. B* **2009**, *79* (24), No. 241103.
(70) Sundararaman, R.; Letchworth-Weaver, K.; Schwarz, K. A.; Gunceler, D.; Ozhabes, Y.; Arias, T. JDFTx: Software for joint density-functional theory. *SoftwareX* **2017**, *6*, 278−284.

(71) Sundararaman, R.; Arias, T. Regularization of the Coulomb singularity in exact exchange by Wigner-Seitz truncated interactions: Towards chemical accuracy in nontrivial systems. *Phys. Rev. B* **2013**, *87* (16), No. 165122.
(72) Garrity, K. F.; Bennett, J. W.; Rabe, K. M.; Vanderbilt, D. Pseudopotentials for high-throughput DFT calculations. *Comput. Mater. Sci.* **2014**, *81*, 446−452.
(73) Hammer, B.; Hansen, L. B.; Nørskov, J. K. Improved adsorption energetics within density-functional theory using revised Perdew-Burke-Ernzerhof functionals. *Phys. Rev. B* **1999**, *59* (11), No. 7413, DOI: 10.1103/PhysRevB.59.7413.
(74) Perdew, J. P.; Burke, K.; Ernzerhof, M. Generalized gradient approximation made simple. *Phys. Rev. Lett.* **1996**, *77* (18), No. 3865, DOI: 10.1103/PhysRevLett.77.3865.
(75) Marques, M. A.; Oliveira, M. J.; Burnus, T. Libxc: A library of exchange and correlation functionals for density functional theory. *Comput. Phys. Commun.* **2012**, *183* (10), 2272−2281.
(76) Gameel, K. M.; Sharafeldin, I. M.; Abourayya, A. U.; Biby, A. H.; Allam, N. K. Unveiling CO adsorption on Cu surfaces: new insights from molecular orbital principles. *Phys. Chem. Chem. Phys.* **2018**, *20* (40), 25892−25900.
(77) Vollmer, S.; Witte, G.; Wöll, C. Determination of site specific adsorption energies of CO on copper. *Catal. Lett.* **2001**, *77* (1), 97−101.
(78) Janthon, P.; Vines, F.; Sirijaraensre, J.; Limtrakul, J.; Illas, F. Adding pieces to the CO/Pt (111) puzzle: the role of dispersion. *J. Phys. Chem. C* **2017**, *121* (7), 3970−3977.
(79) Straumanis, M.; Yu, L. Lattice parameters, densities, expansion coefficients and perfection of structure of Cu and of Cu−In α phase. *Acta Crystallogr., Sect. A* **1969**, *25* (6), 676−682.
(80) Larsen, A. H.; Mortensen, J. J.; Blomqvist, J.; Castelli, I. E.; Christensen, R.; Dułak, M.; Friis, J.; Groves, M. N.; Hammer, B.; Hargus, C.; et al. The atomic simulation environment—a Python library for working with atoms. *J. Phys.: Condens. Matter* **2017**, *29* (27), No. 273002, DOI: 10.1088/1361-648x/aa680e.
(81) Gunceler, D.; Letchworth-Weaver, K.; Sundararaman, R.; Schwarz, K. A.; Arias, T. The importance of nonlinear fluid response in joint density-functional theory studies of battery systems. *Modell. Simul. Mater. Sci. Eng.* **2013**, *21* (7), No. 074005, DOI: 10.1088/0965-0393/21/7/074005.
(82) Sundararaman, R.; Goddard, W. A., III; Arias, T. A. Grand canonical electronic density-functional theory: Algorithms and applications to electrochemistry. *J. Chem. Phys.* **2017**, *146* (11), No. 114104.

https://doi.org/10.1021/acscatal.3c04224
ACS Catal. 2024, 14, 785−796